Am J Cancer Res 2018;8(8):1615-1623
www.ajcr.us /ISSN:2156-6976/ajcr0069384

Original Article

Diffusion MRI biomarkers predict the outcome of irreversible electroporation in a pancreatic tumor mouse model

Matteo Figini[1], Xifu Wang[1,2], Tianchu Lyu[1], Zhanliang Su[1,3], Bin Wang[1,4], Chong Sun[1,5], Junjie Shangguan[1], Liang Pan[1], Kang Zhou[1], Quanhong Ma[1], Vahid Yaghmai[1,6], Daniele Procissi[1], Andrew C Larson[1,6], Zhuoli Zhang[1,6]

[1]Department of Radiology, Feinberg School of Medicine, Northwestern University, Chicago, IL, USA; [2]Department of Radiology, Shanghai General Hospital, Shanghai Jiaotong University, Shanghai, People's Republic of China; [3]Department of Radiology, Tianjin Xiqing Hospital, Tianjin, People's Republic of China; [4]Department of General Surgery, Nanfang Hospital, Southern Medical University, Guangdong Provincial Engineering Technology Research Center of Minimally Invasive Surgery, Guangzhou, People's Republic of China; [5]Department of Orthopedics, Qilu Hospital, Shandong University, Jinan, Shandong, People's Republic of China; [6]Robert H. Lurie Comprehensive Cancer Center, Northwestern University, Chicago, IL, USA

Received November 18, 2017; Accepted November 29, 2017; Epub August 1, 2018; Published August 15, 2018

Abstract: The purpose of this work is to explore the potential contribution of diffusion MRI to predict the effects of irreversible electroporation (IRE) in a pancreatic ductal adenocarcinoma (PDAC) mouse model. Thirteen mice were injected with Panc-02 PDAC cells in both flanks. One tumor was treated with IRE when it reached a diameter of about 5 mm. T2- and diffusion-weighted MRI sequences were acquired before IRE treatment and 1, 3 and 7 days later. The mice were euthanized 1 day (n = 6) or 2 weeks (n = 7) after treatment. The tumors were excised and stained with H&E, caspase-3, CD-3, F4/80. The volume and the mean and standard deviation of the apparent diffusion coefficient (ADC) were compared between treated and untreated lesions and correlated with histology-derived measures. At 1-day post-treatment, a dramatic ADC increase (+50.81%, $P < 0.05$) was found in ablated lesions, strongly correlated with apoptosis ($\tau = 0.90$). At later time points the ADC returned to pre-treatment values, though histopathology showed a quite different scenario compared to the untreated controls. The ADC standard deviation measured within the treated tumors 1 day after IRE treatment had a strong negative correlation with the number of tumor cells found 14 days later ($\tau = 0.80$). There was also a strong correlation between 1-day ADC and 14-day apoptosis in untreated tumors ($\tau = 0.95$). In conclusion, diffusion MRI is sensitive to the short-term effects of IRE in PDAC tumors, and can help predict the long-term treatment outcome.

Keywords: Irreversible electroporation, diffusion MRI, apparent diffusion coefficient, pancreatic cancer, treatment outcome, apoptosis, early prediction, mouse model

Introduction

Pancreatic ductal adenocarcinoma (PDAC) is one of the most aggressive cancers and is the fourth most frequent tumor-related cause of death in the Western world. It is difficult to keep long-term control on locally advanced disease [1]. About a third of patients with PDAC present with locally advanced disease that is not amenable to resection [2]. Systemic chemotherapies and molecularly targeted therapies have offered no or little survival benefit [3]. When surgical options are precluded, image-guided tumor ablation is recommended as the most appropriate therapeutic choice. Conventional ablative therapies (chemical ablation, thermal ablation, and cryoablation) have the potential to be beneficial for locally advanced PDAC [4]. IRE consists in the application of short high-intensity pulses of electric field that create nanopores in the cell membrane and ultimately lead to apoptosis in the target tissue [5]; this mechanism has been known for decades but its application in cancer treatment is relatively recent [6, 7]. IRE represents a new non-thermal injury ablative technique, which

allows definitively treating a soft tissue tumor with a decreased risk of thermal damage to vital structures adjacent to pancreatic tissue [8]. The clinical applications of IRE are growing, especially for liver and pancreatic cancer treatment [9-12].

Non-invasive imaging plays a fundamental role in planning IRE procedures, guiding electrode placement, assessing the treatment effects and detecting complications. Although ultrasound and computed tomography are the most widely used techniques in this context, particularly before and during the intervention, magnetic resonance imaging (MRI) has shown its potential superiority in some studies [13] and is increasingly being utilized for both screening and therapy assessment. However, only T2-weighted and contrast-enhanced T1-weighted sequences are commonly used; the utility of advanced MRI techniques has not been thoroughly investigated [14].

Diffusion MRI (dMRI) is sensitive to water displacement in tissue and thus indirectly to tissue microstructure [15, 16]; dMRI has become popular in research studies and clinical practice, mainly for its sensitivity to many pathological alterations and relative ease of implementation. It may be an ideal candidate for characterizing tumors before and after treatment, but it has been applied in IRE studies only sporadically and with quite diverse protocols and results [13, 17-20]. In particular, one group focused on the change in apparent diffusion coefficient (ADC) shortly after electroporation, but with lower voltage than commonly used and with no validation by histology or other modalities to understand the basis of this alteration [21].

The purpose of our work is to investigate the possibility of characterizing IRE-treated tumors with dMRI and to assess what information it can provide. We studied the ADC time evolution in a pancreatic mouse tumor model after IRE, and we correlated ADC values with histopathology data at both early and late time points after treatment.

Materials and methods

Pancreatic tumor animal model and study timeline

The mouse Panc-02 cell line is derived from amethylcholanthrene-induced PDAC in C57BL/6 mice and was purchased from the American Type Culture Collection (ATCC; Rockville, MD). Panc-02 cells were maintained in RPMI 1640 media (Life Technologies, Carlsbad, CA) supplemented with glutamine (2 mmol/l, Life Technologies), pyruvate (1 mmol/l, Sigma-Aldrich, St. Louis, MO), penicillin and streptomycin (100 IU/ml, Sigma-Aldrich), and 10% fetal bovine serum (FBS, Sigma-Aldrich). The cells were maintained in a humidified atmosphere of 5% CO_2 at 37°C. Before implantation, cell viability was assessed using trypan blue (Sigma-Aldrich) staining (cell viability > 90% was confirmed prior to tumor implantation). Thirteen female C57BL/6 mice (4 weeks of age, weighing between 13 and 17 g) were used for our study. Early-passage Panc-02 cells were harvested and about 2×10^6 cells suspended in 200 µL of phosphate buffered saline (PBS) were subcutaneously implanted into the left and right flanks of each mouse.

All the animals were visually checked every day and underwent checkup MRI at first signs of tumor growth. When the maximum linear size of either tumor reached about 5 mm, a baseline MRI was acquired, and IRE treatment was performed the next day. All the mice underwent MRI again one day after treatment and 6 mice were sacrificed at this time point. The other 7 mice were followed-up for two weeks, with additional MRI scans at 3 and 7 days. Two of these 7 mice had to be terminated after the 7-day MRI for general adverse health conditions; the other 5 mice were sacrificed 14 days after IRE.

Irreversible electroporation

A square-wave Electroporator (ECM830, BTX/Harvard apparatus, Holliston, MA, USA) with a parallel two-needle electrode array was used for all the IRE procedures. The electrode array consisted of two platinum-15% iridium needles inserted in a plastic block with a 5-mm spacing. The IRE ablation protocol, based on our previous studies [22-24], included five 2.5 kV square-wave pulses, with a length of 100 µs and an interval of 100 ms between them. The right-side tumor was treated, unless when it was smaller than 5 mm in diameter and the left-side tumor was larger. The mice were kept under anesthesia with 5% isoflurane in 2 L/minute oxygen during the procedure.

MRI acquisition

MRI experiments were performed on a 7T preclinical scanner (ClinScan, Bruker BioSpin,

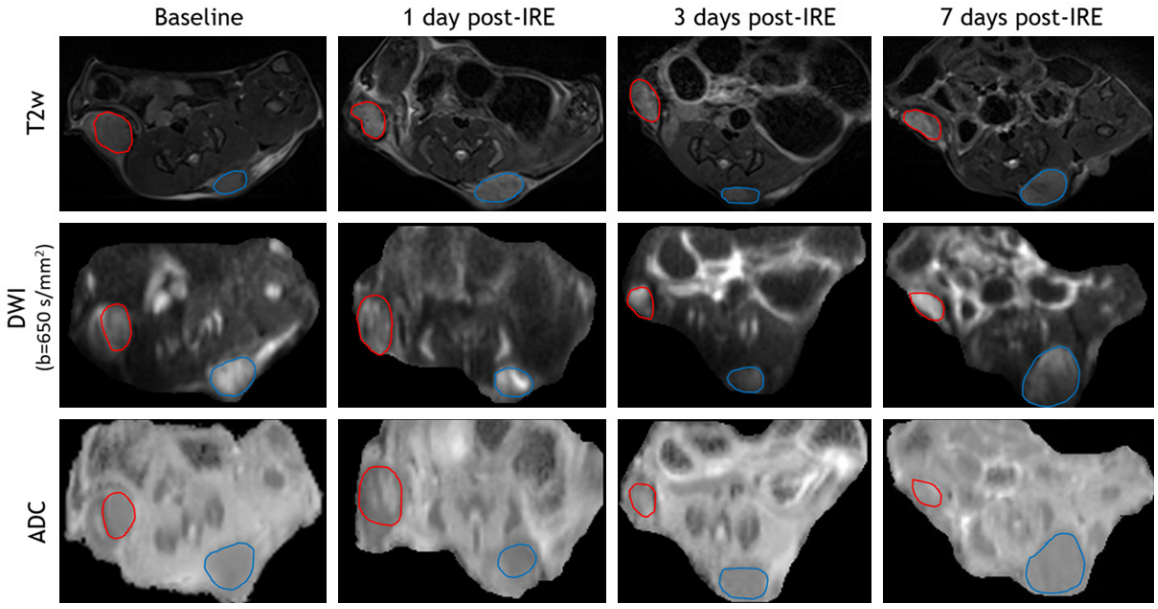

Figure 1. Representative MR images. T2W images, DWI, and ADC maps of baseline, 1 day post-IRE, 3 days post-IRE, and 7 days post-IRE (IRE-treated tumor-red cycle, untreated tumor-blue cycle). These tumor masses were hyperintense (signal intensity is higher than normal muscle signal intensity) within T2W images and DWI images. IRE-treated tumors were typically isointense within ADC maps while untreated tumors were hypointense.

Ettlingen, Germany). The checkup MRI protocol consisted of a coronal (TE = 39 ms, TR = 2750 ms, voxel size = 0.13 × 0.13 × 0.7 mm^3, FOV = 30 × 30 mm^2) and an axial (TE = 40 ms, TR = 4550 ms, voxel size = 0.078 × 0.078 × 0.7 mm^3, FOV = 30 × 30 mm^2) T2-weighted (T2W) sequence.

The baseline and post-treatment scans included the T2W sequences mentioned above and a respiratory-triggered diffusion-weighted imaging (DWI) sequence (TE = 40 ms, TR = 4800 ms, voxel size = 0.3 × 0.3 × 1.5 mm^3, FOV = 30 × 30 mm^2, b = 0, 200, 400, 650, 900, 1200 s/mm^2, 3 orthogonal gradient directions).

MRI processing

The volume of each lesion was measured by manual segmentation of the axial T2W images. A standard mono-exponential model was fitted to the dMRI signal using a custom code in Matlab (Mathworks, Natick, MA, USA):

$$E=\exp(-b\cdot ADC)$$

where b is the b-value (degree of diffusion weighting), E is the dMRI signal normalized to the b = 0 volume, and ADC is the Apparent Diffusion Coefficient, the only free parameter in this model.

Regions of Interest (ROIs) were delineated over the whole tumors on dMRI images and the mean and standard deviation of the ADC within each ROI were calculated. At post-treatment time points, the relative change of the mean ADC compared to baseline was also calculated as:

$$\triangle ADC_{day\_x} = \frac{ADC_{day\_x} - ADC_{baseline}}{ADC_{baseline}}$$

Histopathology

One day (first group) or 14 days (second group) after IRE, the mice were euthanized, and the tumors were excised. Each tumor sample was fixed in 10% formalin, embedded in paraffin, and sliced (5 μm slice thickness). Some slices were placed on glass slides for hematoxylin and eosin (H&E) staining. Other tumor slices were immunostained using antibodies against cleaved caspase-3 (Biocare Medical, Concord, CA) assays by utilizing kits according to the manufacturer's instructions for analysis of apoptotic cell death [25, 26]. The other tumor slices were immunostained using antibodies against CD3 and F4/80 (Biocare Medical, Concord, CA) respectively. The total number of tumor cells (on H&E-stained slices), tumor apoptotic cells (caspase-3 positive cells), T

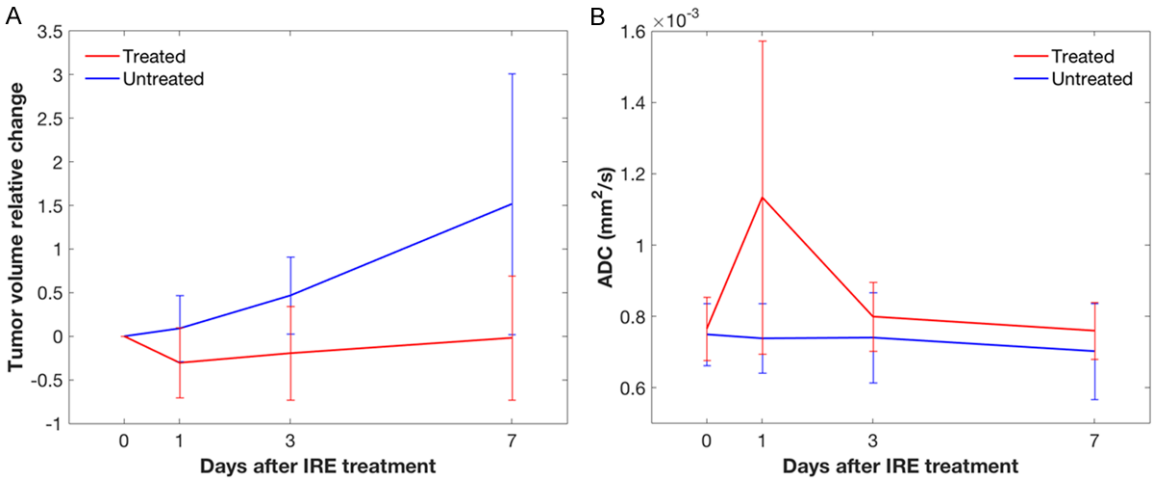

Figure 2. Volume variation and ADC variation after IRE. Relative volume change in treated (red) and untreated (blue) tumors at baseline (0 days), 1, 3 and 7 days after IRE; the error bars represent the standard deviation across the 7 studied mice, showing a high variability in both groups (A). Mean ADC in treated (red) and untreated (blue) tumors at baseline (0 days), 1, 3 and 7 days after IRE; the error bars represent the standard deviation across the 7 studied mice, showing a high variability especially in treated lesions at 1 day (B).

cells (CD3 positive cells) and macrophage cells (F4/80 positive cells) were counted under microscopy in 5 views (× 20) for each control or IRE-treated tumor. All counts were performed by two investigators (Drs. ZZ and QM, with more than 10 years of experience) using a double-headed light microscope.

Statistical analysis

The mean, standard deviation, and relative change of the ADC at each time point were compared between treated and untreated tumors using a Wilcoxon signed-rank test. Within each of the groups of lesions, the same parameters at each post-treatment timepoint were also compared to the corresponding baseline values using a Wilcoxon signed-rank test. A *p*-value lower than 0.05 was considered significant for all the comparisons. The correlation between the dMRI parameters at each time point and the number of tumor cells, apoptotic cells, T cells, macrophages or the MRI-derived relative volume change 7 days after IRE was evaluated with Kendall's tau.

Results

MRI findings

T2W images, DWI (b = 650 s/mm^2), and ADC maps of baseline, 1 day post-IRE, 3 days post-IRE, and 7 days post-IRE (IRE treated tumor-red cycle, untreated tumor-blue cycle) are shown in **Figure 1**. These tumor masses were consistently hyperintense within T2W images and DWI images. IRE-treated tumors were typically isointense within ADC maps while untreated tumors were hypointense.

Based on tumor volume measurement using T2w images, all the untreated tumors grew with time, from 40.47 ± 17.16 mm^3 at baseline to 82.22 ± 39.22 mm^3 at 7 days. The treated tumors decreased on average, from 79.29 ± 97.44 mm^3 at baseline, to 70.60 ± 92.79 mm^3 at 7 days post-treatment (**Figure 2A**), but the variability was high and 3 out of 7 treated lesions increased in volume.

The mean and standard deviation of the ADC remained constant in the untreated tumors, with no statistically significant difference at any time point compared to the baseline scan except a slight decrease at 7 days (P = 0.0469). The mean ADC in treated tumors 1 day after IRE was significantly higher than at baseline (P = 0.0156) and also compared with the untreated tumor at 1 day (P = 0.0012) (**Figure 2B**).

Histopathology

Representative histology sections corresponding to the untreated and treated lesions in the same mouse are shown in **Figure 3**. The first and second rows are untreated and IRE-treated

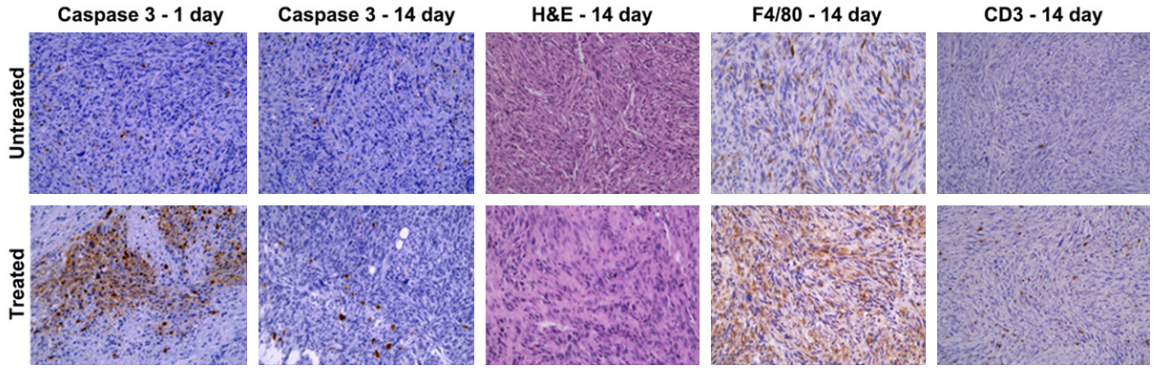

Figure 3. Representative histology sections. Sections corresponding to the untreated and treated lesions in the same mouse are shown in the first and second row respectively, whereas each column corresponds to a different staining (Caspase 3-1 and 14 days after IRE, H&E, F4/80 and CD3). Image magnification is 40 × for all panels. Extensive apoptosis is evident at 1 day and no more visible at 14 days in treated tumors; a lower number of tumor cells, as well as a higher number of macrophages and T cells, are present at 14 days in treated tumors.

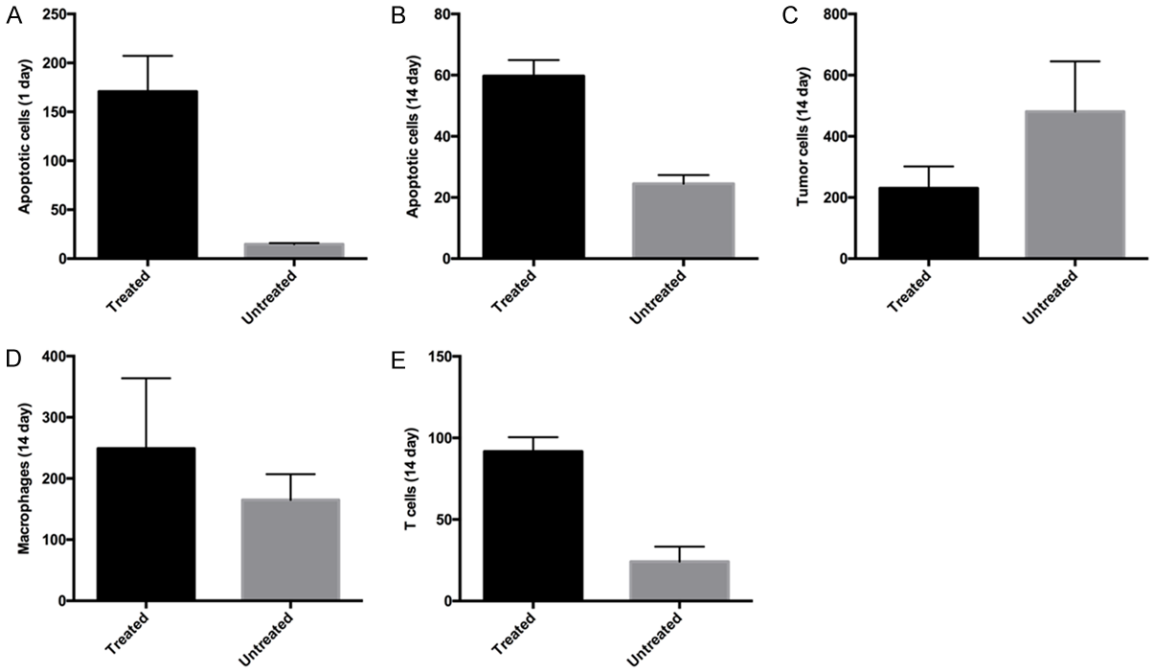

Figure 4. Histology quantitative results. Number of apoptotic cells (caspase-3 staining), tumor cells (H&E staining), macrophages (F4/80 staining) and T cells (CD3 staining) found in treated and untreated lesions. The values are shown as mean ± SD across the different mice. There was significantly extensive apoptosis between treated and untreated tumors at 1 day ($P = 0.008$) (A) and 14 days ($P = 0.008$) (B). There was a lower number of tumor cells in treated lesions comparing untreated lesions at 14 days post-IRE ($P = 0.016$) (C), as well as a higher number of macrophages (D) and T cells (E) are present at 14 days in treated tumors comparison with those of untreated tumors (macrophage, treated vs. untreated $P = 0.04$; T cell, treated vs. untreated $P = 0.008$).

tumors respectively, whereas each column corresponds to a different staining (Caspase-3 1 and 14 days after IRE, H&E, F4/80 and CD3). Image magnification is 40 × for all panels.

At 1 day post-IRE, extensive activation of caspase-3 was shown in treated tumors compared to untreated tumors in the same mice. At 14 days post-IRE, the caspase-3 activation was no longer visible over a necrotic background across the entire lesion, but the number of apoptotic cells was still significantly higher than in untreated tumors. At 14 days we also found a significantly lower number of tumor cells (H&E

Table 1. Correlation results in treated tumors

	ADC-1 day			ADC-7 days		
	Mean	Mean % change	SD	Mean	Mean % change	SD
Apoptotic cells-1 day	+0.70	+0.90	+0.70	-	-	-
Apoptotic cells-14 days	+0.00	+0.60	-0.80	-1.00	-0.40	-0.60
Tumor cells-14 days	+0.40	+0.60	-0.80	-0.60	-0.40	-0.60
T cells-14 days	-0.20	-0.80	+0.60	+0.80	+0.20	+0.80
Macrophages-14 days	-0.60	0.00	-0.20	-0.40	+0.20	0.00

Kendall's tau values obtained in treated tumors for the correlations between the histology-derived quantitative measures specified in each row and the mean value (mean), the relative difference between the mean value and the baseline mean value (mean % change), and the standard deviation (SD) of the ADC measured at 1 day (first 3 columns) or at 7 days (last 3 columns).

Table 2. Correlation results in untreated tumors

	ADC-1 day			ADC-7 days		
	Mean	Mean % change	SD	Mean	Mean % change	SD
Apoptotic cells-1 day	-0.20	+0.30	0.00	-	-	-
Apoptotic cells-14 days	+0.95	+0.11	+0.74	+0.74	+0.74	-0.11
Tumor cells-14 days	-0.40	+0.40	-0.20	-0.60	-0.20	-0.40
T cells-14 days	+0.20	-0.20	0.00	+0.40	0.00	+0.20
Macrophages-14 days	+0.20	-0.20	0.00	+0.40	0.00	+0.20

Kendall's tau values obtained in untreated tumors for the correlations between the histology-derived quantitative measures specified in each row and the mean value (mean), the relative difference between the mean value and the baseline mean value (mean % change), and the standard deviation (SD) of the ADC measured at 1 day (first 3 columns) or at 7 days (last 3 columns).

staining) and a significantly higher number of T cells in treated tumors when compared with untreated tumors (CD3 staining), whereas the number of macrophages (F4/80 staining) was trending to be higher but this difference did not achieve statistical significance with current sample size (**Figure 4**).

Correlation between the ADC and histopathology measurements

The results of all the correlations between the dMRI-derived and histology-derived measures are reported in **Tables 1** and **2** for treated and untreated lesions respectively. The most relevant results will be described below.

In the treated tumors, there was a strong correlation between the ADC relative change 1 day after treatment and the number of apoptotic cells at the same time point. Also, the mean and standard deviation of the ADC at 1 day had a correlation, though weaker, with the number of apoptotic cells at 1 day. By contrast, there was no evident correlation in untreated tumors at this early time point.

In untreated tumors there was a moderate positive correlation between the mean ADC measured at 7 days and the number of apoptotic cells at 14 days. In treated tumors, the mean ADC measured 7 days after IRE had a strong negative correlation with the number of apoptotic cells, and a positive correlation with the number of T-cells found at 14 days. There was also a strong correlation between the within-ROI standard deviation of the ADC measurements in the treated tumors at 7 days and the number of T-cells found at 14 days.

When the 1-day dMRI and the 14-day histology data were compared in the treated lesions, the strongest correlations (all negative) were found between the 1-day ADC change and the number of T-cells and between the ADC standard deviation and the number of apoptotic and tumor cells.

In untreated tumors, a positive correlation was found between the ADC mean and standard deviation at 1 day and the number of apoptotic cells at 14 days.

By contrast, the MRI-derived volume change at 7 days had only a weak negative correlation with the ADC relative change at 1 day in treated tumors (τ = -0.62) and even weaker correlations with the other dMRI values at 1 day (data not shown).

Discussion

We studied the effect of IRE treatment in a murine pancreatic cancer model with longitudinal ADC measurements, correlated with histopathology data at both early and late time points.

We observed a transient dramatic increase of the mean ADC in tumors treated with IRE 1 day

after the procedure and a return to pre-treatment values as early as 2 days later. The few previous studies applying dMRI after IRE treatment did not examine multiple non-acute times, and reported contradictory results, particularly in preclinical studies. Rat models showed no effect on dMRI [19] or an ADC increase 5 to 25 minutes after electroporation [21], while mouse models showed an ADC increase 30 minutes after IRE [20] or an ADC reduction 1 and 3 hours after treatment followed by progressive normalization at 6 and 24 hours [18]. In patients, one study found an ADC decrease for the first 24 hours after the procedure, followed by an increase above the pre-treatment values 1 to 12 months later [17]; another study found no significant differences in ADC 1 to 6 months after IRE [13]. The different extent and timing of the multiple mechanisms involved in the response to IRE treatment could explain the observed discrepancies.

We found a very strong correlation between the 1-day ADC change in treated tumors and the number of apoptotic cells measured at 1 day, suggesting that this dramatic ADC increase may be driven mostly by apoptosis.

At later time points, the ADC in untreated tumors correlated positively with apoptosis and negatively, though weakly, with the number of tumor cells, as expected and shown by many studies [27]. On the other hand, the ADC in treated tumors showed not only a weak negative correlation with the number of tumor cells, similar to untreated tumors, but also a positive correlation with the number of T cells and, surprisingly, a very strong negative correlation with apoptosis. Thus, the ADC in treated tumors may depend upon different factors than in the untreated tumors. Even though the values are very similar in the two groups, the tumor microenvironment is probably quite different and in fact the observed ADC normalization was not a sign of return to normal conditions. Further analysis would be needed to derive more detailed and specific conclusions.

The most intriguing results are those associating the 1-day ADC with long-term histopathology data. In treated tumors, the ADC relative change 1 day after treatment was positively correlated with the number of T cells found 14 days after treatment, so the ADC increase is apparently a biomarker of poor tumor response, even though it is associated with the degree of apoptosis at 1 day; the weak correlation between the 1-day relative ADC change and the number of tumor cells somewhat supports this unexpected result, but further studies are needed for confirmation.

The ADC standard deviation within the treated tumors had a strong negative correlation with the number of tumor cells and a weaker positive correlation with the number of T cells at 14 days. It had also a negative correlation with the number of apoptotic cells, but apoptosis occurs primarily in the acute post-treatment stage and is not a mechanism of primary importance in the sub-acute phases, as shown by comparing our 1-day and 14-days measurements. Thus, according to our results, tumors with a less homogeneous ADC 1 day after IRE tend to respond better to the treatment.

An unexpected result of this study is the strong correlation found in untreated tumors between the ADC at 1 day (approximately 2 weeks after tumor cell injection) and the number of apoptotic cells at 14 days (approximately 1 month after tumor cell injection). This suggests that the microstructural information provided by the ADC could help predict the natural evolution of the tumors. Prior studies have sought to develop mathematical models to predict tumor growth based on MRI, but most of these have only estimated the future tumor volume [28-30], whereas our results suggest that even microstructural and functional features could be predicted. Future studies should investigate this possibility, applying multiple MRI techniques and correlating quantitative MRI parameters at early time points with histopathological data at late time points, similarly to the work of Ng et al. [31].

The main limitation of this study was the relatively low number of animals used in each group, which might have limited the statistical significance of the analysis. Moreover, we selected relatively few time points and found statistically significant differences only 1 day after treatment; additional acute MRI acquisitions may have improved insights into tumor response to IRE. However, no previous work has attained such a thorough longitudinal MRI time-course after IRE with both early and late histopathology correlations. We believe that our study represents a necessary step towards

a better understanding of IRE treatment effects. Nonetheless, more detailed analyses should be performed in the future to confirm and refine our results.

In conclusion, we described a transient dramatic ADC increase, strongly correlated with apoptosis, one day after IRE treatment in mouse pancreatic tumors. At later time points the ADC returned to pre-treatment values, while histopathological data showed quite different features and a different relation between these measurements and the ADC in treated and untreated pancreatic tumors. We also showed that dMRI could be an early non-invasive method to predict response to IRE treatment of pancreatic cancer, as well as the microstructural evolution of untreated tumors.

Acknowledgements

This work was supported by grants R01CA-196967 and R01CA209886 funded by the USA National Cancer Institute (National Institutes of Health).

Disclosure of conflict of interest

None.

Address correspondence to: Dr. Zhuoli Zhang, Robert H. Lurie Comprehensive Cancer Center, Department of Radiology, Feinberg School of Medicine, Northwestern University, 737 N. Michigan Ave, 16th Floor, Chicago 60611, IL, USA. Tel: 312-926-3874; Fax: 312-926-5991; E-mail: zhuolizhang@northwestern.edu; Dr. Daniel Procissi, Department of Radiology, Feinberg School of Medicine, Northwestern University, Chicago, IL, USA. Tel: 312-503-2247; Fax: 312-926-5991; E-mail: d-procissi@northwestern.edu

References

[1] Perez K, Clancy TE, Mancias JD, Rosenthal MH and Wolpin BM. When, what, and why of perioperative treatment of potentially curable pancreatic adenocarcinoma. J Clin Oncol 2016; [Epub ahead of print].

[2] Sohal DP, Mangu PB, Khorana AA, Shah MA, Philip PA, O'Reilly EM, Uronis HE, Ramanathan RK, Crane CH, Engebretson A, Ruggiero JT, Copur MS, Lau M, Urba S and Laheru D. Metastatic pancreatic cancer: American society of clinical oncology clinical practice guideline. J Clin Oncol 2016; 34: 2784-2796.

[3] Barton MK. Germline mutations in pancreatic cancer become better defined. CA Cancer J Clin 2016; 66: 93-94.

[4] Wolfgang CL, Herman JM, Laheru DA, Klein AP, Erdek MA, Fishman EK and Hruban RH. Recent progress in pancreatic cancer. CA Cancer J Clin 2013; 63: 318-348.

[5] Weaver JC. Electroporation theory. Concepts and mechanisms. Methods Mol Biol 1995; 55: 3-28.

[6] Davalos RV, Mir IL and Rubinsky B. Tissue ablation with irreversible electroporation. Ann Biomed Eng 2005; 33: 223-231.

[7] Miller L, Leor J and Rubinsky B. Cancer cells ablation with irreversible electroporation. Technol Cancer Res Treat 2005; 4: 699-705.

[8] Sutter O, Calvo J, N'Kontchou G, Nault JC, Ourabia R, Nahon P, Ganne-Carrie N, Bourcier V, Zentar N, Bouhafs F, Sellier N, Diallo A and Seror O. Safety and efficacy of irreversible electroporation for the treatment of hepatocellular carcinoma not amenable to thermal ablation techniques: a retrospective single-center case series. Radiology 2017; 284: 877-886.

[9] Lencioni R, Crocetti L and Narayanan G. Irreversible electroporation in the treatment of hepatocellular carcinoma. Tech Vasc Interv Radiol 2015; 18: 135-139.

[10] Bhatia SS, Arya R and Narayanan G. Niche applications of irreversible electroporation. Tech Vasc Interv Radiol 2015; 18: 170-175.

[11] Lyu T, Wang X, Su Z, Shangguan J, Sun C, Figini M, Wang J, Yaghmai V, Larson AC and Zhang Z. Irreversible electroporation in primary and metastatic hepatic malignancies: a review. Medicine (Baltimore) 2017; 96: e6386.

[12] Moir J, White SA, French JJ, Littler P and Manas DM. Systematic review of irreversible electroporation in the treatment of advanced pancreatic cancer. Eur J Surg Oncol 2014; 40: 1598-1604.

[13] Granata V, de Lutio di Castelguidone E, Fusco R, Catalano O, Piccirillo M, Palaia R, Izzo F, Gallipoli AD and Petrillo A. Irreversible electroporation of hepatocellular carcinoma: preliminary report on the diagnostic accuracy of magnetic resonance, computer tomography, and contrast-enhanced ultrasound in evaluation of the ablated area. Radiol Med 2016; 121: 122-131.

[14] Figini M, Wang X, Lyu T, Su Z, Procissi D, Yaghmai V, Larson AC and Zhang Z. Preclinical and clinical evaluation of the liver tumor irreversible electroporation by magnetic resonance imaging. Am J Transl Res 2017; 9: 580-590.

[15] Le Bihan D. Molecular diffusion, tissue microdynamics and microstructure. NMR Biomed 1995; 8: 375-386.

[16] Le Bihan D and Iima M. Diffusion magnetic resonance imaging: what water tells us about

biological tissues. PLoS Biol 2015; 13: e1002203.
[17] Barabasch A, Distelmaier M, Heil P, Kramer NA, Kuhl CK and Bruners P. Magnetic resonance imaging findings after percutaneous irreversible electroporation of liver metastases: a systematic longitudinal study. Invest Radiol 2017; 52: 23-29.
[18] Calmels L, Al-Sakere B, Ruaud JP, Leroy-Willig A and Mir LM. In vivo MRI follow-up of murine tumors treated by electrochemotherapy and other electroporation-based treatments. Technol Cancer Res Treat 2012; 11: 561-570.
[19] Hjouj M, Last D, Guez D, Daniels D, Sharabi S, Lavee J, Rubinsky B and Mardor Y. MRI study on reversible and irreversible electroporation induced blood brain barrier disruption. PLoS One 2012; 7: e42817.
[20] Zhang Z, Li W, Procissi D, Tyler P, Omary RA and Larson AC. Rapid dramatic alterations to the tumor microstructure in pancreatic cancer following irreversible electroporation ablation. Nanomedicine (Lond) 2014; 9: 1181-1192.
[21] Mahmood F, Hansen RH, Agerholm-Larsen B, Jensen KS, Iversen HK and Gehl J. Diffusion-weighted MRI for verification of electroporation-based treatments. J Membr Biol 2011; 240: 131-138.
[22] Guo Y, Zhang Y, Klein R, Nijm GM, Sahakian AV, Omary RA, Yang GY and Larson AC. Irreversible electroporation therapy in the liver: longitudinal efficacy studies in a rat model of hepatocellular carcinoma. Cancer Res 2010; 70: 1555-1563.
[23] Guo Y, Zhang Y, Nijm GM, Sahakian AV, Yang GY, Omary RA and Larson AC. Irreversible electroporation in the liver: contrast-enhanced inversion-recovery MR imaging approaches to differentiate reversibly electroporated penumbra from irreversibly electroporated ablation zones. Radiology 2011; 258: 461-468.
[24] Zhang Y, Guo Y, Ragin AB, Lewandowski RJ, Yang GY, Nijm GM, Sahakian AV, Omary RA and Larson AC. MR imaging to assess immediate response to irreversible electroporation for targeted ablation of liver tissues: preclinical feasibility studies in a rodent model. Radiology 2010; 256: 424-432.
[25] Roy SK, Chen Q, Fu J, Shankar S and Srivastava RK. Resveratrol inhibits growth of orthotopic pancreatic tumors through activation of FOXO transcription factors. PLoS One 2011; 6: e25166.
[26] Cheng G, Zhu L and Mahato RI. Caspase-3 gene silencing for inhibiting apoptosis in insulinoma cells and human islets. Mol Pharm 2008; 5: 1093-1102.
[27] Chen L, Liu M, Bao J, Xia Y, Zhang J, Zhang L, Huang X and Wang J. The correlation between apparent diffusion coefficient and tumor cellularity in patients: a meta-analysis. PLoS One 2013; 8: e79008.
[28] Hormuth DA 2nd, Weis JA, Barnes SL, Miga MI, Rericha EC, Quaranta V and Yankeelov TE. A mechanically coupled reaction-diffusion model that incorporates intra-tumoural heterogeneity to predict in vivo glioma growth. J R Soc Interface 2017; 14.
[29] Hormuth DA 2nd, Weis JA, Barnes SL, Miga MI, Rericha EC, Quaranta V and Yankeelov TE. Predicting in vivo glioma growth with the reaction diffusion equation constrained by quantitative magnetic resonance imaging data. Phys Biol 2015; 12: 046006.
[30] Fujima N, Sakashita T, Homma A, Harada T, Shimizu Y, Tha KK, Kudo K and Shirato H. Non-invasive prediction of the tumor growth rate using advanced diffusion models in head and neck squamous cell carcinoma patients. Oncotarget 2017; 8: 33631-33643.
[31] Ng TSC, Wert D, Sohi H, Procissi D, Colcher D, Raubitschek AA and Jacobs RE. Serial diffusion MRI to monitor and model treatment response of the targeted nanotherapy CRLX101. Clin Cancer Res 2013; 19: 2518-2527.